Nonlinearity effects on the directed momentum current

Wen-Lei Zhao,[1,2,3] Li-Bin Fu,[2,3,*] and Jie Liu[2,3,†]

[1]*School of Science, Jiangxi University of Science and Technology, Ganzhou 341000, China*

[2]*National Laboratory of Science and Technology on Computational Physics, Institute of Applied Physics and Computational Mathematics, Beijing 100088, China*

[3]*HEDPS, Center for Applied Physics and Technology, Peking University, Beijing 100084, China*

(Received 25 June 2013; revised manuscript received 26 January 2014; published 14 August 2014)

We investigate the quantum transport dynamics governed by the nonlinear Schrödinger equation with a periodically-δ-kicking potential and discover the emergence of a directed current in momentum space. With the increase of nonlinearity, we find strikingly that the momentum current decreases, reverses, and finally vanishes, indicating that the quantum transport can be effectively manipulated through adjusting the nonlinearity. The underlying dynamic mechanism is uncovered and some important implications are addressed.

DOI: 10.1103/PhysRevE.90.022907 PACS number(s): 05.45.−a, 05.60.Gg, 37.10.Jk

I. INTRODUCTION

Nonlinear quantum systems, where the dynamics is governed by nonlinear Schrödinger equations, have become increasingly prominent in physics. They often arise in the mean field treatment of many-body quantum systems, such as Bose-Einstein condensates (BECs) of dilute atomic gases [1,2], and as a possible fundamental nonlinear modification of quantum mechanics [3]. Other applications of such modification include nonlinear light propagation [4] and Ginzburg-Landau equations for complex order parameters in condensed-matter physics.

The emergence of nonlinearity means that the Hamiltonian is the functional of an instantaneous wave function, which breaks the superposition principle of quantum mechanics [5]. The nonlinearity can dramatically alter the quantum dynamics of tunneling [6], interference [7], and the associated quantum phases [8]. For instance, due to the nonlinearity arising from an atomic interaction, the quantum tunneling of the coherent atoms in a double-well potential was found to be suppressed or totally restrained, leading to the striking self-trapping phenomenon [9,10], as was observed in recent BEC experiments [11]. Recent studies have been extended to quantum transport governed by nonlinear Schrödinger equations [4,12,13], where the nonlinear effects are also prominent.

Among these studies, the directed transport of particles with unbiased external forces [14,15] is of particular interest as its mechanism is relevant for the construction of nanoscale devices, such as particle separation and electron pumps, and for the understanding of biological molecular motors [16–19]. Cold-atom experiments have demonstrated such striking phenomena [20]. However, the study of the nonlinear effect on the quantum ratchet transport is in the initial stage [21–24] and the question of how the nonlinearity affects the quantum directed transport calls for thorough investigation both theoretically and experimentally.

In this paper we investigate the nonlinearity effects on the directed transport both analytically and numerically, with a focus on the momentum current in the quantum resonance case of periodically driven systems. For the noninteracting case, the momentum current may grow indefinitely and linearly with time or oscillate around a mean value clearly different from zero [25]. We investigate the directed transport in the presence of both quantum resonance and nonlinearity and find the unbounded linear growth of the momentum current with time. More interesting is that increases in nonlinearity can reduce, reverse, and finally stop the directed momentum current. In the presence of nonlinearity, the wave-packet bifurcates into two portions in momentum space. Each portion can be well approximated by a coherent state (CS) that is periodically revived. The temporal-spatial evolution of the wave packet indicates a clear modification of the Talbot-type recurrence by nonlinearity. With an increase of nonlinearity, the CSs are squeezed into Fock states in momentum space that impedes the directed momentum current. The system we studied is realizable in experiments, for example, in an ultracold-coherent-atom system (i.e., a BEC) [26–29]. We therefore hope our theoretical results will stimulate future experiments in the fields.

The paper is organized as follows. In Sec. II we describe the system and show the momentum current in the presence of nonlinearity. In Sec. III we show the wave-packet dynamics, e.g., the formation of CSs, and its directed motion in momentum space. In Sec. IV we present a summary.

II. DIRECTED MOMENTUM CURRENT UNDER NONLINEARITY

The system considered here is BEC atoms confined in a ring trap of radius R and thickness r with $r \ll R$. As the lateral motion of the atoms is negligible, the system is essentially one dimensional [29]. The BEC atoms experience periodic δ kicks induced by an optical standing wave. The dynamics of the system is described by the dimensionless nonlinear Gross-Pitaevskii equation ($\hbar = 1$)

$$i\frac{\partial}{\partial t}\psi(\theta,t) = \left(-\frac{1}{2}\frac{\partial^2}{\partial\theta} + K\cos(\theta)\delta_T + g|\psi|^2\right)\psi(\theta,t), \tag{1}$$

where $g = \frac{8NaR}{r^2}$ is the scaled strength of the nonlinear interaction, N is the number of BEC atoms, a is the s-wave

*lbfu@iapcm.ac.cn

†liu_jie@iapcm.ac.cn

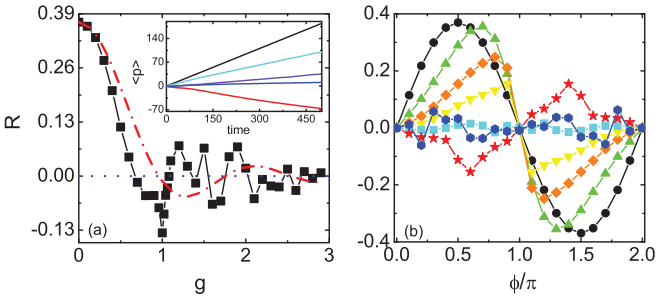

FIG. 1. (Color online) (a) Acceleration rate R versus g for $\phi = \frac{\pi}{2}$ and $K = 0.74$. The red dash-dotted line indicates the theoretical prediction in Eq. (2). The blue dotted line denotes the saturation level. The inset shows the time dependence of $\langle p \rangle$. From top to bottom $g = 0$ (black line), 0.4 (cyan line), 1.5 (violet line), 2 (blue line), and 1 (red line). Time is measured in the number of kick periods ($T = 4\pi$). (b) Plot of R versus $\frac{\phi}{\pi}$ for $K = 0.74$ with $g = 0$ (black circles), 0.3 (green up triangles), 0.5 (orange diamonds), 0.6 (yellow down triangles), 0.7 (cyan squares), 1 (red pentagrams), and 2 (blue hexagons).

scattering length, K is the kick strength, $\delta_T = \sum_n \delta(t - nT)$, and T is the period of kicks. The length and the energy are measured in units R and $\frac{\hbar^2}{mR^2}$, respectively. The wave function normalization reads $\int_0^{2\pi} |\psi(\theta)|^2 d\theta = 1$ and the boundary condition is periodic $\psi(\theta,t)=\psi(\theta + 2\pi,t)$.

The system has spatial and time-reversal symmetries, in which the emergence of the directed transport requires the rectification of kicking force that can be realized by setting an asymmetric initial wave packet. Experimentally using the Bragg pulse, one can prepare a superposition state of the form $\psi_0(\theta) = \frac{1}{\sqrt{4\pi}}(1 + e^{i(\phi-\theta)})$ with a relative phase factor ϕ [26]. When $g = 0$, this quantum state can be revived exactly at a period duration of the Talbot time ($T = 4\pi$) [30], i.e., the quantum resonance phenomenon [31]. In this situation, the average momentum takes the form $\langle p(t) \rangle = \langle p_0 \rangle + \frac{K}{2} \sin(\phi)t$, where $\langle p_0 \rangle$ is the initial value [26]. The average momentum is found to grow linearly with time, indicating the emergence of directed current in momentum space with the growth rate (or acceleration [25]) of $R = \frac{d\langle p \rangle}{dt} = \frac{K}{2} \sin(\phi)$.

In order to investigate the momentum current under the influence of nonlinearity, we solve the nonlinear Schrödinger equation numerically using split-operator method [32]. The inset in Fig. 1(a) shows that, for weak nonlinearity (e.g., $g = 0.4$), the linear growth rate of the momentum current decreases compared to that in the noninteracting case. With an increase of the nonlinearity to $g = 1$, the momentum current reverses direction and its linear growth rate becomes negative. For a higher nonlinearity of $g = 1.5$, the momentum current is again in the positive direction while the acceleration becomes very slow. At a strong nonlinearity of $g = 2$, the momentum current almost vanishes. The above observations are more clearly demonstrated in Fig. 1(a), in which the accelerations R decreases from 0.37 ($=\frac{K}{2}$) to a negative value -0.13, oscillates, and finally converges at zero after $g = 3$. Our theoretical prediction of the growth rate is

$$R = \frac{K}{2}[J_0(4g) + J_2(4g)] \sin(\phi), \qquad (2)$$

where J_0 and J_2 are zeroth and second order Bessel functions, respectively (for details see Appendixes A–C). The results are compared with numerical results and show a qualitative coincidence, as shown in Fig. 1(a).

The accelerations show a strong dependence of the phase. In Fig. 1(b) we plot the dependence of R on ϕ for varied g. We see that, with the increase of nonlinearity, the amplitude of acceleration gradually decreases and at $g = 2$ the R oscillates around zero with very small amplitudes, indicating the complete suppression of the momentum current by strong nonlinearity. For any g, the momentum currents are found to vanish at the phases of 0, π, and 2π, coinciding with our theoretical prediction of Eq. (2). The physics behind this behavior is the parity mismatch between the density distribution and the kicking force. At $\phi = n\pi$, the density distribution during temporal evolution maintains even parity with respect to $\theta = 0$, while the force that is the derivative of the potential is an odd function. We then expect the average force to be zero and the directed momentum current vanishes.

The dependence of the acceleration rate on ϕ reveals that the symmetry breaking between the kicking potential and the density distribution leads to the directed current of the BEC atoms. Such spontaneous symmetry breaking also results in the directed motion of the soliton in the classical Frenkel-Kontorova model [33,34]. In the traditional study of ratchet transport, the driven potential is spatially asymmetric. For such systems, the mechanism of the directed current of particles is different from that of the spontaneous symmetry breaking.

III. WAVE-PACKET DYNAMICS

To achieve insight into the mechanism of the nonlinear momentum current, we trace the temporal evolution of the wave packet in both the momentum and coordinate spaces. The results are shown in Fig. 2. For $g = 0$, the wave packet spreads along the positive momentum direction [Figs. 2(a) and 2(b)], corresponding to the linear growth of the directed current. When the nonlinearity is present (i.e., $g = 0.5$), the wave packet in momentum space bifurcates into two portions that move in opposite directions linearly as time evolves [Fig. 2(c)] and the momentum distribution exhibits two sharp peaks [Fig. 2(d)]. In this situation, the movement of one portion of BEC atoms to negative momentum results in the reduction of the momentum current. At a higher nonlinearity of $g = 1.0$ [Figs. 2(e) and 2(f)], the two portions of BEC atoms move in opposite directions initially, but after $t_c \simeq 100$ they all move to negative momentum, which leads to the current reversal. For adequately strong nonlinearity, our extensive investigations show that the wave packet always has one prominent peak whose location does not change with time, e.g., $g = 3$ in Figs. 2(g) and 2(h). In this case, the directed momentum current vanishes.

The corresponding states in coordinate space are shown in Fig. 3. In the noninteracting case, the periodic revival of the quantum state, i.e., the temporal Talbot effect, can be seen in Figs. 3(a) and 3(b). Interestingly, for weak nonlinearity, e.g., $g = 0.5$ in Figs. 3(c) and 3(d), the time evolution of the probability density distribution exhibits the periodic pattern

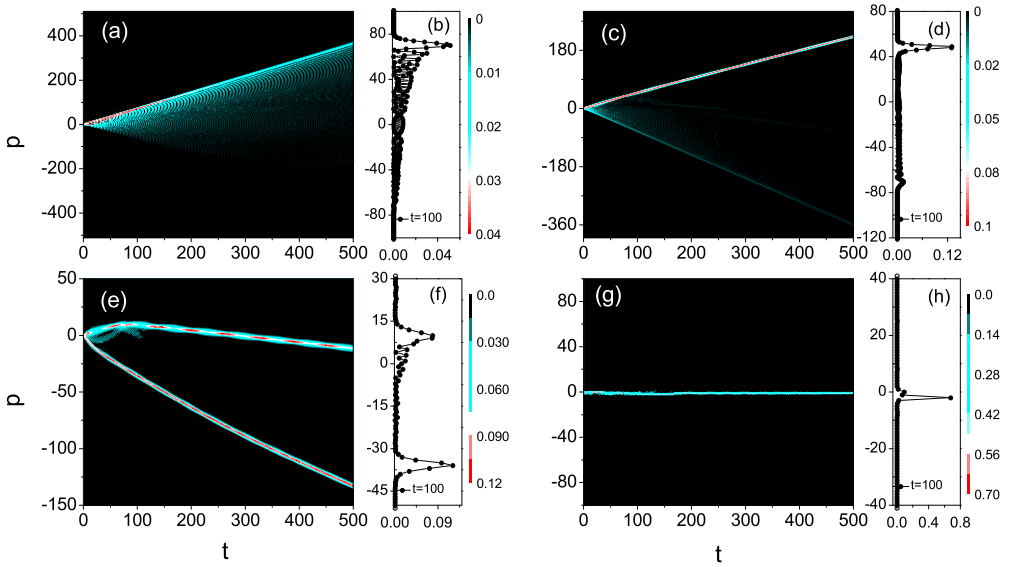

FIG. 2. (Color online) Time evolution of the probability density distribution in the momentum space for $g = 0$ (a), 0.5 (c), 1.0 (e), and 3.0 (g). (b), (d), (f), and (h) Plots of the momentum distribution at $t = 100$ for $g = 0$, 0.5, 1.0, and 3.0, respectively. Other parameters are the same as in Fig. 1(a).

whose period is much larger than the kick period, indicating the modification of the Talbot-type recurrence by nonlinearity. For much larger nonlinearity, e.g., $g = 1$ in Figs. 3(e) and 3(f), the *space-time* evolution of the wave packet exhibits a complicated interference pattern. For adequately strong nonlinearity, e.g., $g = 3$ in Figs. 3(g) and 3(h), the wave packet wildly spreads in the coordinate space, corresponding to the extreme squeeze of the quantum state in momentum space.

We further calculate the phase space distribution of the quantum state, i.e., the Husimi distribution $|\langle\psi|\Phi\rangle|^2$, where $|\Phi\rangle$ is a CS centered at (θ_c, p_c), with $\langle\theta|\Phi\rangle = (\frac{\lambda_c}{\pi})^{1/4} \exp[-\frac{\lambda_c}{2}(\theta-\theta_c)^2 + ip_c\theta]$. Its spreading width in coordinate space is $1/2\lambda_c$. In our numerical implementation, we set $\lambda_c = 5$. In the noninteracting case ($g = 0$), the quantum state is $\psi(\theta,t) = \psi(\theta,0)e^{-iKt\cos(\theta)}$. The corresponding Husimi distribution is approximated as

$$|\langle\psi|\Phi\rangle|^2 \approx \left(\frac{4}{\lambda\pi}\right)^{1/2} J_N^2(Kt)\exp\left[-\frac{(p_0 \mp N)^2}{\lambda}\right] \times [1 \pm \sin(\phi)][1+\sin(\theta_0)], \quad (3)$$

where $J_N(Kt)$ is the Bessel function and N equals the magnitude of its argument Kt, i.e., $N \approx Kt$ (for details see Appendixes A–C). One can see that for $\phi = \pi/2$, the maximum of the quantum phase space distribution corresponds to $\theta_0 = \pi/2$ and $p_0 = N$, which is confirmed by the numerical results in Figs. 4(a) and 4(b).

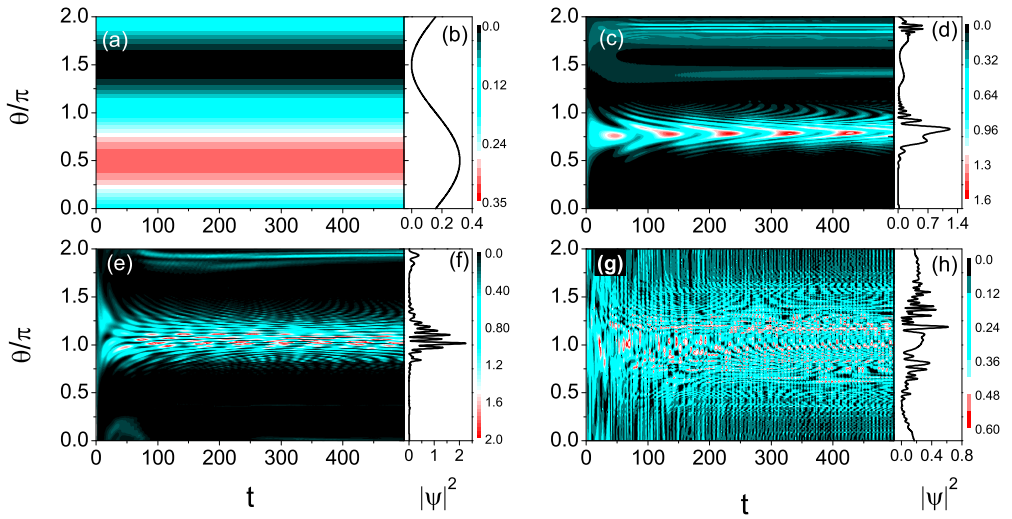

FIG. 3. (Color online) Time evolution of the probability density distribution in the coordinate space for $g = 0$ (a), 0.5 (c), 1.0 (e), and 3.0 (g). (b), (d), (f), and (h) Plots of the probability density distribution at $t = 100$ for $g = 0$, 0.5, 1.0, and 3.0, respectively. Other parameters are the same as in Fig. 1(a).

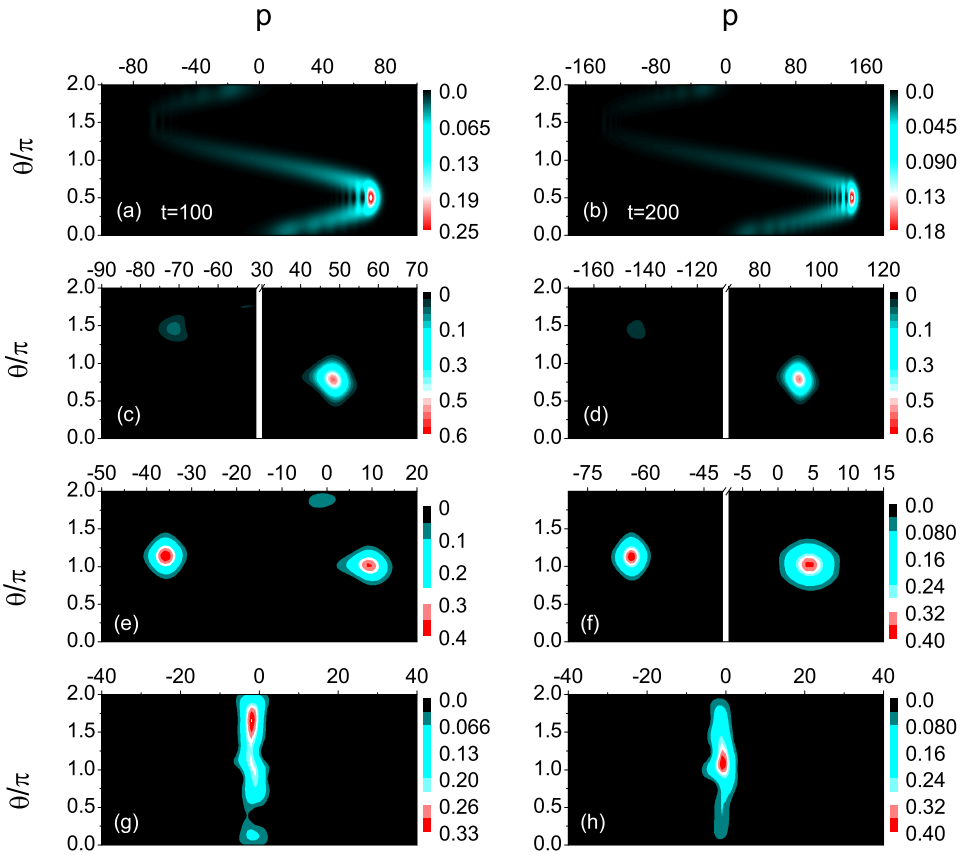

FIG. 4. (Color online) Husimi distributions $|\langle\psi|\Phi\rangle|^2$ at time $t = 100$ (left panels) and 200 (right panels) for, from top to bottom, $g = 0$, 0.5, 1.0, and 3.0, respectively. Other parameters are the same as in Fig. 1(a).

For weak nonlinearity, the wave packet in the momentum space consists of two fractions $\psi(p) = \psi_1(p) + \psi_2(p)$. Our numerical investigations show that each one has the Gaussian configuration

$$\psi_n(p) = \sqrt{\rho_n}\exp\left[-\frac{1}{2\lambda_n}\left(p - p_0^n\right)^2 - i\left(p - p_0^n\right)\theta_0^n\right]$$

$(n = 1,2)$, where ρ_n is the probability amplitude, λ_n characterizes the width, p_0^n and θ_0^n are the centers of the Gaussian state. The corresponding Husimi distribution is $|\langle\psi|\Phi\rangle|^2 \approx \sum_{n=1}^{2}|\langle\psi_n|\Phi\rangle|^2$, where

$$|\langle\psi_n|\Phi\rangle|^2 = \sqrt{\frac{\pi}{\lambda_c}}\frac{2\rho_n}{\gamma_n}\exp\left[-\frac{\left(\theta_c - \theta_0^n\right)^2}{\gamma_n} - \frac{\left(p_c - p_0^n\right)^2}{\lambda_n + \lambda_c}\right],$$

with $\gamma_n = \frac{1}{\lambda_n} + \frac{1}{\lambda_c}$ (for details see Appendixes A–C). The quantum interference between $\langle\psi_n|\Phi\rangle$ is vanishingly small due to the large distance between the two fractions, i.e., $|p_0^1 - p_0^2| \gg 1$. Thus, the Husimi distribution consists of two separating CSs, which is confirmed by the numerical results in Figs. 4(c)–4(f). Detailed observations show that, for $g = 0.5$ in Figs. 4(c) and 4(d), each CS is centered at a fixed coordinate, while it moves to positive momentum for the significant fragment or negative momentum for the small one, respectively. For stronger nonlinearity, e.g., $g = 1$ in Figs. 4(e) and 4(f), the two fragments of the Husimi distribution are comparable and they all move to negative momentum. They fully overlap in coordinate space, which results in the interference pattern [see Fig. 3(e)]. For adequately strong nonlinearity, e.g., $g = 3$ in Figs. 4(g) and 4(h), the Husimi distribution is localized at a fixed momentum and spreads wildly along the coordinate variable, indicating the formation of the Fock state.

For a complete understanding of the dynamics of the CSs, we numerically investigate the values of the parameters $(\rho,\lambda,\theta_0,p_0)$ for a wild range of g and time. We numerically find that the wave packets consist of two CSs for g smaller than a critical value $g_c \simeq 1.08$ and one significant CS for $g > g_c$ [see Figs. 2(e)–2(g)]. The insets in Figs. 5(a) and 5(b) show that, for a specific g, both the probability amplitude ρ and the width λ of the CSs are stable with time evolution, demonstrating the stability of the CSs. The time-averaged value $\langle\rho\rangle_t$ as a function of g is shown in Fig. 5(a), where we can see the quite fast growth of the left CS with g. More interesting is that the time-averaged values of $\langle\lambda\rangle_t$ rapidly decrease with the increase of g, as shown in Fig. 5(b), which demonstrates the process of the squeezed CSs (for details see Appendixes A–C).

The motion of the CS can be well characterized by the time dependence of its center (θ_0, p_0). The inset in Fig. 5(c) shows that, for a specific g, the θ_0 of each CS is almost a constant with time evolution. Interestingly, the time-averaged value of $\langle\theta_0\rangle_t$ of the left (right) CS gradually decreases (increases) to π with the increase of g, and $\langle\theta_0\rangle_t \approx \pi$ for $g > g_c$, as shown in Fig. 5(c). The center θ_0 determines the driven force $\langle F\rangle = K\langle\sin(\theta)\rangle$ that the BEC atoms experience from the periodic kicks. Such force is negative (positive) for $\theta_0 > \pi$

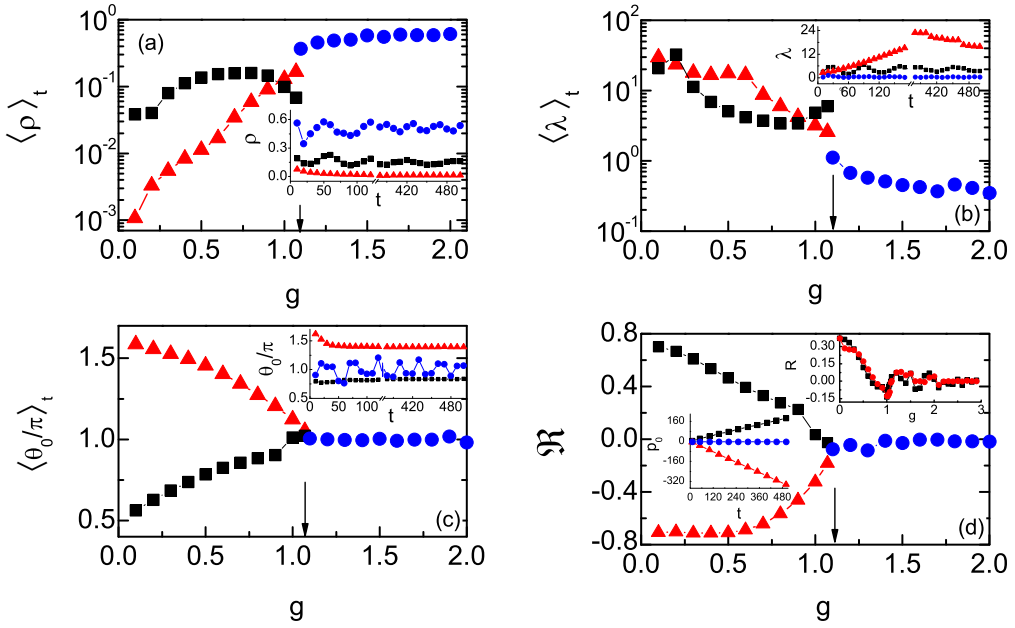

FIG. 5. (Color online) Time averaged value of the parameters $(\rho,\lambda,\theta_0,p_0)$ of the CS versus g. Arrows mark the critical nonlinearity $g_c \simeq 1.08$. For $g < g_c$, black squares (red triangles) correspond to the right (left) CSs. The insets in (a)–(c) show the time dependence of ρ, λ, and θ_0 for $g = 0.6$ and 1.4. The insets in (d) show p_0 versus t with $g = 0.6$ and 1.4 (left) and the comparison of the acceleration rate $\tilde{R}$ (red circles) with R (black squares) (right). Other parameters are the same as in Fig. 1(a).

($<\pi$) and zero for $\theta_0 = \pi$, which results in the move of the CSs in different directions. This is confirmed by the numerical results in the inset in Fig. 5(d), which displays the linear decrease or increase of p_0 for the two CSs for $g = 0.6$ and the nonincrease of p_0 for $g = 1.4$. The main plot of Fig. 5(d) shows the acceleration rate $\Re = \lim_{t\to+\infty} p_0/t$ of each CS for a wide range of g. We see that the acceleration rates of the two CSs approach zero as g increases to g_c, beyond which $\Re = 0$. We assume that the acceleration rate of the momentum current is approximated as $\tilde{R} = \langle\rho\rangle_t^l \Re^l + \langle\rho\rangle_t^r \Re^l$, where the superscript r (l) denotes the right (left) CSs. The inset in Fig. 5(d) shows that the $\tilde{R}$ agrees well with the acceleration rate R of the real system, demonstrating the control of the directed momentum current by the movement of the CSs.

IV. SUMMARY

We have investigated both numerically and analytically the quantum resonance ratchets of periodically kicked BECs in the presence of the nonlinearity. Our theoretical prediction of the generation of the momentum current is in good agreement with numerical results. Nonlinear interactions are shown to induce the consecutive reversals of the directed momentum current, which is different from the current reversal in Refs. [35,36] where the growth of momentum current saturates as time evolves. Our detailed numerical results show that the movement of the CSs controls the directed current of the BEC atoms. The CSs are squeezed with the increase of the nonlinearity and turn into a Fock state in momentum space for adequately strong nonlinearity. The results are within the reach of the cold-atom experiments [26–29].

ACKNOWLEDGMENTS

We are grateful to Dr. W. Wang for stimulating discussions. This work was supported by the NFRP (Grants No. 2011CB921503, No. 2013CBA01502, and No. 2013CB834100) and the NNSF of China (Grants No. 91021021 and No. 11274051).

APPENDIX A: DERIVATION OF THE GROWTH RATE OF MOMENTUM CURRENT

We analytically derive the quantum state after the nonlinear evolution of period T, i.e., $\psi(T^-,\theta)$, where the minus sign superscript denotes the time immediately before the first kick. It is obtained by approximately separating the nonlinear evolution between consecutive kicks into two time intervals, i.e., $\Delta t = \frac{T}{2}$. For the time evolution of the state in each interval, we use the split operator method only one time. Then, after the first interval the quantum state is described as

$$\psi(\theta,\Delta t) = \exp\left(-i\frac{p^2}{2}\frac{\Delta t}{2}\right)\exp\left[-i\left|\tilde{\psi}\left(\frac{\Delta t}{2},\theta\right)\right|^2\Delta t\right] \times \exp\left(-i\frac{p^2}{2}\frac{\Delta t}{2}\right)\psi(\theta,0),$$

where $\psi(\theta,0) = 1/\sqrt{2\pi}$ denotes the initial state and $\tilde{\psi}(\frac{\Delta t}{2},\theta) = \exp(-i\frac{p^2}{2}\frac{\Delta t}{2})\psi(\theta,0)$. For the quantum resonance $T = 4\pi$, the time interval equals $\frac{\Delta t}{2} = 4\pi\frac{1}{4}$. Thus, the free evolution in such a time interval belongs to the high-order

quantum resonance case, i.e., $T = 4\pi\frac{p}{q}$ with $p = 1$ and $q = 4$. In the general case, i.e., $T = 4\pi\frac{p}{q}$, there is an analytical expression for the quantum state $\tilde{\psi}(T,\theta)$,

$$\tilde{\psi}(\theta,T) = \sum_{n=0}^{q-1} C_n \psi\left(\theta + 2\pi\frac{n}{q},0\right),$$

with $C_n = \frac{1}{q}\sum_{m=0}^{q-1}\exp(-i\frac{2\pi p}{q}m^2 - i\frac{2\pi mn}{q})$ [31].

By using the above equation, we can obtain the analytical formula of $\psi(\theta,\Delta t)$. By repeating this step for the second time interval, we can obtain the state at the time $t = T^-$,

$$\psi(\theta,T^-) \simeq e^{-i2g}\exp[-iK\cos(\theta)]\{\cos[2g\cos(\theta)]\psi(\theta,0) + \sin[2g\cos(\theta)]\psi(\theta+\pi,0)\}.$$

According to the above expression, we can calculate the growth rate of the momentum current and regard it as the average acceleration, considering that the momentum current is almost linearly growing with time. It then reads

$$R = \frac{K}{2}[J_0(4g) + J_2(4g)]\sin(\phi), \tag{A1}$$

where J_0 and J_2 are Bessel functions of the zeroth and the second kind, respectively.

APPENDIX B: DERIVATION OF HUSIMI DISTRIBUTION OF THE BEC WAVE PACKETS

1. Husimi distribution for the linear case $g = 0$

The Husimi distribution of the quantum state is $|\langle\psi|\Phi\rangle|^2$, where $|\Phi\rangle$ is a CS centered at (θ_c,p_c), with $\langle\theta|\Phi\rangle = (\frac{\lambda_c}{\pi})^{1/4}\exp[-\frac{\lambda_c}{2}(\theta-\theta_c)^2 + ip_c\theta]$. Its spreading width in coordinate space is $1/2\lambda_c$. In the noninteracting case, i.e., $g = 0$, the quantum state is $\psi(\theta,t) = \psi_0(\theta)e^{-iKt\cos(\theta)}$. The corresponding inner product $\langle\psi|\Phi\rangle$ takes the form

$$\langle\psi|\Phi\rangle = \frac{e^{-ip_0\theta_0}}{(4\pi\lambda_c)^{1/4}}\sum_{n=-\infty}^{+\infty}[J_n(Kt) - ie^{i\phi}J_{n+1}(Kt)]G_n, \tag{B1}$$

where $G_n = \exp[-\frac{(n-p_0)^2}{2\lambda_c} + in\theta]$ and $J_n(Kt)$ is the Bessel function. We see that the quantum phase space distribution exhibits the interference of the Gaussian wave packets. The Bessel function $|J_n(Kt)|$ is about maximum when n equals the magnitude of its argument Kt, which we mark as N, i.e., $|n| \approx N$, and exponentially decreases, i.e., $J_n(Kt) \to 0$ as n departs from N. Thus, we can safely conclude that the sum on the right-hand of Eq. (B1) involves only the terms with $|n| = N$ and $N-1$. In this situation, the Husimi distribution is approximated as

$$|\langle\psi|\Phi\rangle|^2 \approx \left(\frac{4}{\lambda\pi}\right)^{1/2}J_N^2(Kt)\exp\left[-\frac{(p_0\mp N)^2}{\lambda}\right] \times [1\pm\sin(\phi)][1+\sin(\theta_0)].$$

One can see that for $\phi = \pi/2$, the maximum of the quantum phase space distribution corresponds to $\theta_0 = \pi/2$ and $p_0 = N$, which is confirmed by our numerical results.

2. Husimi distribution for the nonlinear case $g \neq 0$

Our numerical results show that, for moderate strength of nonlinearity, the wave packets consist of two fractions in momentum space, i.e., $\psi(p) = \psi_1(p) + \psi_2(p)$ $(n = 1,2)$. Moreover, each fraction can be well described by the Gaussian state [see Eq. (5)]

$$\psi_n(p) = \sqrt{\rho_n}\exp\left[-\frac{1}{2\lambda}\left(p - p_0^n\right)^2 - i\left(p - p_0^n\right)\theta_0^n\right].$$

The inner product between $|\psi_n\rangle$ and the CS $|\Phi\rangle$ is

$$\langle\psi_n|\Phi\rangle = \left(\frac{\pi}{\lambda_c}\right)^{1/4}\sqrt{\frac{2\rho_n}{\gamma_n}}\exp\left[-\frac{\left(\theta_c-\theta_0^n\right)^2}{2\gamma_n} - \frac{\left(p_c-p_0^n\right)^2}{2(\lambda_n+\lambda_c)} + i\phi_n\right],$$

where $\gamma_n = \frac{1}{\lambda_n} + \frac{1}{\lambda_c}$ and $\phi_n = (p_c - p_0^n)[(1 + \frac{1}{\gamma_n\lambda_n})\theta_0^n - \frac{\theta_c}{\gamma_n\lambda_n}]$. For the total wave function $\psi(p) = \psi_1(p) + \psi_2(p)$, the Husimi distribution has the expression

$$|\langle\psi|\Phi\rangle|^2 = \sum_{n=1}^{2}|\langle\psi_n|\Phi\rangle|^2 + 2\,\mathrm{Re}(\langle\psi_1|\Phi\rangle^*\langle\psi_2|\Phi\rangle),$$

where $\mathrm{Re}(\cdots)$ denotes the real part of the complex number and reflects the quantum interference

$$\mathrm{Re}(\langle\psi_1|\Phi\rangle^*\langle\psi_2|\Phi\rangle) = 2\left(\frac{\pi}{\lambda_c}\right)^{1/2}\left\{\prod_{n=1}^{2}\sqrt{\frac{\rho_n}{\gamma_n}}\exp\left[-\frac{\left(\theta_c-\theta_0^n\right)^2}{2\gamma_n} - \frac{\left(p_c-p_0^n\right)^2}{2(\lambda_n+\lambda_c)}\right]\right\}\cos(\phi_1-\phi_2).$$

On condition that $|p_0^1 - p_0^2| \gg 0$, this term is nearly zero. Thus, the Husimi distribution consists of two CSs, i.e., $|\langle\psi|\Phi\rangle|^2 \approx \sum_{n=1}^{2}|\langle\psi_n|\Phi\rangle|^2$.

APPENDIX C: SQUEEZE OF THE CS BY THE NONLINEARITY

For the system of the periodically kicked BEC on a ring, the quantum state can be expanded in terms of the eigenstates of the angular momentum operators, namely, $|\psi\rangle = \psi_n|n\rangle$, where $p|n\rangle = n|n\rangle$. For $g = 0$, Eq. (1) describes the quantum kicked rotor model. For this model, the mapping equation of the Fourier coefficients ψ_n from t to $(t+1)$ is

$$\psi_n(t+1) = \sum_m(-i)^{n-m}J_{n-m}(k)\psi_m(t)\exp\left(-i\frac{T}{2}m^2\right). \tag{C1}$$

Here and in the following, t is measured in the number of periods.

For the BEC system that is described by Eq. (1), it is hard to analytically treat the time evolution of the quantum state. In Ref. [37] Shepelyansky introduced an approximation for the nonlinearity, i.e., $g|\psi(\theta)|^2 \sim g|\psi_n|^2/(2\pi)$, and called this model the kicked nonlinear rotor (KNR). For such a model,

the mapping equation of ψ_n is

$$\psi_n(t+1) = \sum_m (-i)^{n-m} J_{n-m}(k)\psi_m(t) \times \exp\left(-i\frac{T}{2}m^2 - i\tilde{g}|\psi_n|^2 T\right), \quad \text{(C2)}$$

where $\tilde{g} = g/2\pi$. In Ref. [38] Rebuzzini *et al.* numerically investigated energy diffusion in quantum resonance and found ballistic diffusion in the presence of nonlinearity, which demonstrates that the wave-packet dynamics of the quantum KNR mimics that of the BEC system in Eq. (1). Taking this into account, we use the KNR model to analyze the effect of nonlinearity on time evolution of the wave packet. We show the mechanism of squeezing of the CSs by nonlinearity.

In the linear case ($g = 0$), the wave packet is periodically revived when the kick period is the Talbot time $T = 4\pi$. The origin is that the phase factor of the free evolution term is unity $\exp(-i4\pi m^2/2) = 1$, so free evolution has no effect on the wave-packet motion. It is easy to see that the free evolution for $T = 4\pi$ is equal to that for $T = 0$. Taking this into account, Eq. (C2) is rewritten as

$$\begin{aligned}\psi_{t+1}(p) &= \exp[-i\tilde{g}|\psi_t(p)|^2 T]\psi_t(p) \\ &= \exp[-i\bar{g}|\psi_t(p)|^2]\psi_t(p), \end{aligned} \quad \text{(C3)}$$

where $\bar{g} = 2g$, and for the simplicity of the theoretical analysis, we use the continuous variable p to replace the discrete one n. The above equation can be further described by

$$\begin{aligned}\psi_{t+1}(p) &= \exp[-i\bar{g}|\psi_t(p)|^2]\psi_t(p) \\ &= \left\{1 + \sum_{n=1}^{+\infty}\frac{1}{n!}[-i\bar{g}|\psi_t(p)|^2]^n\right\}\psi_t(p) \\ &= \psi_t(p) + \sum_n \frac{1}{n!}(-i\bar{g})^n|\psi_t(p)|^{2n}\psi_t(p). \end{aligned} \quad \text{(C4)}$$

Our numerical investigations show that the wave packets in momentum space can be well described by the CSs. Thus, in the following we consider how the CSs change during the time evolution in Eq. (C4). A CS in momentum space takes the form ($\hbar = 1$)

$$\psi(p) = \left(\frac{1}{\lambda\pi}\right)^{1/4} \exp\left[-\frac{1}{2\lambda}(p-p_0)^2 - ix_0(p-p_0)\right]. \quad \text{(C5)}$$

The modular square of such a wave packet is $|\psi(p)|^2 = (\frac{1}{\lambda\pi})^{1/2}\exp[-\frac{1}{\lambda}(p-p_0)^2]$. It is easy to see that $|\psi(p)|^{2n} = (\frac{1}{\lambda\pi})^{n/2}\exp[-\frac{n}{\lambda}(p-p_0)^2]$, which is also a Gaussian wave packet. For such a state the product $|\psi(p)|^{2n}\psi(p)$ takes the form

$$\begin{aligned}|\psi(p)|^{2n}\psi(p) &= \left(\frac{1}{\lambda\pi}\right)^{n/2}\exp\left[-\frac{n}{\lambda}(p-p_0)^2\right]\left\{\left(\frac{1}{\lambda\pi}\right)^{1/4} \times \exp\left[-\frac{1}{2\lambda}(p-p_0)^2 - ix_0(p-p_0)\right]\right\} \\ &= \left(\frac{1}{\lambda\pi}\right)^{n/2}\left(\frac{1}{\lambda\pi}\right)^{1/4} \times \exp\left[-\frac{1}{2\lambda_n}(p-p_0)^2 - ix_0(p-p_0)\right] \\ &= \left(\frac{1}{\lambda\pi}\right)^{n/2}\left(\frac{\lambda_n}{\lambda}\right)^{1/4}\psi_n(p), \end{aligned} \quad \text{(C6)}$$

where $\lambda_n = \frac{\lambda}{2n+1}$, and the CS $\psi_n(p)$ is

$$\psi_n(p) = \left(\frac{1}{\lambda_n\pi}\right)^{1/4}\exp\left[-\frac{1}{2\lambda_n}(p-p_0)^2 - ix_0(p-p_0)\right]. \quad \text{(C7)}$$

Inserting Eq. (C6) into Eq. (C4) yields the time evolution of the CS $\psi(p)$,

$$\tilde{\psi}(p) = \psi(p) + \sum_{n=1}^{+\infty}\frac{1}{n!}(-i\bar{g})^n\left(\frac{1}{\lambda\pi}\right)^{n/2}\left(\frac{\lambda_n}{\lambda}\right)^{1/4}\psi_n(p), \quad \text{(C8)}$$

where we use the state $\tilde{\psi}(p)$ to replace $\psi_{t+1}(p)$. The last term on the right-hand side of the above equation denotes the effect of the nonlinearity. The width of $\psi_n(p)$ in momentum space is $\Delta_p^n = \lambda_n/2 = \frac{\lambda}{2(2n+1)}$. Since $n > 1$, it is smaller than $\lambda/2$, which is the width of $\psi(p)$. Therefore, the CS $\psi^n(p)$ is squeezed in the presence of nonlinearity. It seems possible, in principle, to show that $\tilde{\psi}(p)$ is squeezed compared to $\psi(p)$.

[1] F. Dalfovo and S. Giorgini, Rev. Mod. Phys. **71**, 463 (1999); A. J. Leggett, *ibid.* **73**, 307 (2001).

[2] L. P. Pitaevskii and S. Stringari, *Bose-Einstein Condensation* (Oxford University Press, New York, 2003).

[3] S. Weinberg, Phys. Rev. Lett. **62**, 485 (1989); Ann. Phys. (NY) **194**, 336 (1989); B. Mielnik, Commun. Math. Phys. **37**, 221 (1974).

[4] Y. Lahini, F. Pozzi, M. Sorel, R. Morandotti, D. N. Christodoulides, and Y. Silberberg, Phys. Rev. Lett. **101**, 193901 (2008); Y. Silberberg and B. G. Sfez, Opt. Lett. **13**, 1132 (1988).

[5] Y. S. Kivshar and B. A. Malomed, Rev. Mod. Phys. **61**, 763 (1989); Y. B. Band, B. Malomed, and M. Trippenbach, Phys. Rev. A **65**, 033607 (2002).

[6] M. Grifoni and P. Hänggi, Phys. Rep. **304**, 229 (1998); A. Smerzi, S. Fantoni, S. Giovanazzi, and S. R. Shenoy, Phys. Rev. Lett. **79**, 4950 (1997).

[7] Y. Shin, M. Saba, T. A. Pasquini, W. Ketterle, D. E. Pritchard, and A. E. Leanhardt, Phys. Rev. Lett. **92**, 050405 (2004); T. Schumm, S. Hofferberth, L. M. Andersson, S. Wildermuth, S. Groth, I. Bar-Joseph, J. Schmiedmayer, and P. Krüger, Nat. Phys. **1**, 57 (2005).

[8] J. Liu, B. Wu, and Q. Niu, Phys. Rev. Lett. **90**, 170404 (2003); J. Liu, B. Hu, and B. Li, *ibid.* **81**, 1749 (1998); J. Liu, W. Wang, C. Zhang, Q. Niu, and B. Li, Phys. Rev. A **72**, 063623 (2005); J. Liu and L. B. Fu, *ibid.* **81**, 052112 (2010); B. Wu, J. Liu, and Q. Niu, Phys. Rev. Lett. **94**, 140402 (2005).

[9] G. J. Milburn, J. Corney, E. M. Wright, and D. F. Walls, Phys. Rev. A **55**, 4318 (1997); L. Salasnich, *ibid.* **61**, 015601 (1999); S. Kohler and F. Sols, Phys. Rev. Lett. **89**, 060403 (2002).

[10] G. F. Wang, L. B. Fu, and J. Liu, Phys. Rev. A **73**, 013619 (2006); B. Wang, P. Fu, J. Liu, and B. Wu, *ibid.* **74**, 063610 (2006).

[11] M. Albiez, R. Gati, J. Fölling, S. Hunsmann, M. Cristiani, and M. K. Oberthaler, Phys. Rev. Lett. **95**, 010402 (2005).

[12] T. Kottos and M. Weiss, Phys. Rev. Lett. **93**, 190604 (2004); A. S. Pikovsky and D. L. Shepelyansky, *ibid.* **100**, 094101 (2008); S. Flach, D. O. Krimer, and Ch. Skokos, *ibid.* **102**, 024101 (2009).

[13] F. Benvenuto, G. Casati, A. S. Pikovsky, and D. L. Shepelyansky, Phys. Rev. A **44**, R3423 (1991).

[14] R. P. Feynman, R. B. Leighton, and M. Sands, *The Feynman Lectures on Physics* (Addison-Wesley, Reading, 1966), Vol. 1, Chap. 46.

[15] P. Reimann, Phys. Rep. **361**, 57 (2002); P. Hänggi and F. Marchesoni, Rev. Mod. Phys. **81**, 1 (2009).

[16] S. Kohler, J. Lehmann, and P. Hänggi, Phys. Rep. **406**, 379 (2005).

[17] F. Jülicher, A. Ajdari, and J. Prost, Rev. Mod. Phys. **69**, 1269 (1997).

[18] R. D. Astumian, Science **276**, 917 (1997); R. D. Astumian and P. Hänggi, Phys. Today **55**(11), 33 (2002).

[19] J. Lehmann, S. Kohler, P. Hänggi, and A. Nitzan, Phys. Rev. Lett. **88**, 228305 (2002).

[20] F. Renzoni, Contemp. Phys. **46**, 161 (2005); Adv. At. Mol. Opt. Phys. **57**, 1 (2009).

[21] D. Poletti, G. Benenti, G. Casati, and B. Li, Phys. Rev. A **76**, 023421 (2007); D. Poletti, G. Benenti, G. Casati, P. Hänggi, and B. Li, Phys. Rev. Lett. **102**, 130604 (2009); G. G. Carlo, G. Benenti, G. Casati, S. Wimberger, O. Morsch, R. Mannella, and E. Arimondo, Phys. Rev. A **74**, 033617 (2006); G. G. Carlo, G. Benenti, G. Casati, and D. L. Shepelyansky, Phys. Rev. Lett. **94**, 164101 (2005).

[22] O. Romero-Isart and J. J. García-Ripoll, Phys. Rev. A **76**, 052304 (2007).

[23] L. Morales-Molina and S. Flach, New J. Phys. **10**, 013008 (2008).

[24] E. Lundh and M. Wallin, Phys. Rev. Lett. **94**, 110603 (2005); E. Lundh, Phys. Rev. E **74**, 016212 (2006).

[25] A. Kenfack, J. Gong, and A. K. Pattanayak, Phys. Rev. Lett. **100**, 044104 (2008); D. Y. H. Ho and J. Gong, *ibid.* **109**, 010601 (2012); J. Wang and J. B. Gong, Phys. Rev. A **77**, 031405(R) (2008); J. Gong and P. Brumer, Phys. Rev. E **70**, 016202 (2004).

[26] M. Sadgrove, M. Horikoshi, T. Sekimura, and K. Nakagawa, Phys. Rev. Lett. **99**, 043002 (2007).

[27] I. Dana, V. Ramareddy, I. Talukdar, and G. S. Summy, Phys. Rev. Lett. **100**, 024103 (2008); I. Dana and V. Roitberg, Phys. Rev. E **76**, 015201(R) (2007).

[28] G. J. Duffy, S. Parkins, T. Müller, M. Sadgrove, R. Leonhardt, and A. C. Wilson, Phys. Rev. E **70**, 056206 (2004); C. Ryu, M. F. Andersen, A. Vaziri, M. B. d'Arcy, J. M. Grossman, K. Helmerson, and W. D. Phillips, Phys. Rev. Lett. **96**, 160403 (2006).

[29] C. Zhang, J. Liu, M. G. Raizen, and Q. Niu, Phys. Rev. Lett. **92**, 054101 (2004).

[30] L. Deng, E. W. Hagley, J. Denschlag, J. E. Simsarian, M. Edwards, C. W. Clark, K. Helmerson, S. L. Rolston, and W. D. Phillips, Phys. Rev. Lett. **83**, 5407 (1999).

[31] F. M. Izrailev and D. L. Shepelyanskii, Theor. Math. Phys. **43**, 553 (1980).

[32] A. D. Bandrauk and H. Shen, J. Phys. A **27**, 7147 (1994); B. Hu, B. Li, J. Liu, and Y. Gu, Phys. Rev. Lett. **82**, 4224 (1999).

[33] L. L. Bonilla and B. A. Malomed, Phys. Rev. B **43**, 11539 (1991); B. A. Malomed, Phys. Rev. A **45**, 4097 (1992).

[34] A. V. Ustinov and B. A. Malomed, Phys. Rev. B **64**, 020302(R) (2001).

[35] M. Sadgrove and S. Wimberger, New J. Phys. **11**, 083027 (2009).

[36] R. K. Shrestha, J. Ni, W. K. Lam, S. Wimberger, and G. S. Summy, Phys. Rev. A **86**, 043617 (2012).

[37] D. L. Shepelyansky, Phys. Rev. Lett. **70**, 1787 (1993).

[38] L. Rebuzzini, S. Wimberger, and R. Artuso, Phys. Rev. E **71**, 036220 (2005).